INTERNATIONAL JOURNAL FOR NUMERICAL METHODS IN FLUIDS, VOL. 4, 749–764 (1984)

SOME EXPLICIT TRIANGULAR FINITE ELEMENT SCHEMES FOR THE EULER EQUATIONS

FRANÇOISE ANGRAND AND ALAIN DERVIEUX

INRIA, Institut National de Recherche en Informatique et en Automatique, Domaine de Voluceau Rocquencourt, B.P. 105, 78153 Le Chesnay Cedex, France

SUMMARY

Several explicit schemes are presented for *triangular* P_0 and P_1 *finite elements*. A first-order accurate upwind P_0 scheme is compared to a FLIC type method. A second-order accurate Richtmyer scheme is constructed. Applications are given for the Euler system of conservation laws in the 2-dimensional case.

KEY WORDS Hyperbolic Conservation Equation Finite Elements

INTRODUCTION

In this paper we are dealing with *finite element simulation* of perfect fluid flows. The choice of finite element methods is interesting because it provides facilities in mesh generation around complex geometries. The flexibility and reliability of such an approach has now been proved by transonic simulations with a finite element full potential model.[1]

Some *explicit* and *low-order* (first and second) accurate unsteady methods are presented here to solve the Euler equations.

For the first-order case, P_0 approximations (constant by triangles) have been experimented with; the comparison between the number of degrees of freedom and the cost of computation is particularly favourable to this choice. Unfortunately, a general stability analysis seems non-trivial.

For the second order case, a P_1 (continuous, linear by triangles) approximation is used to construct a two-dimensional two-step Richtmyer scheme. Linear stability is studied in the scalar case by the energy approach.

UPWIND METHOD FOR F.E.M.

The equations

The basic equations for two-dimensional inviscid compressible flows are described as follows:

$$\frac{\partial W}{\partial t}+\frac{\partial}{\partial x}F(W)+\frac{\partial}{\partial y}G(W)=0 \tag{1}$$

where

$$W=\begin{pmatrix}\rho\\ \rho u\\ \rho v\\ e\end{pmatrix},\qquad F(W)=\begin{pmatrix}\rho u\\ \rho u^2+p\\ \rho uv\\ (e+p)u\end{pmatrix},\qquad G(W)=\begin{pmatrix}\rho v\\ \rho uv\\ \rho v^2+p\\ (e+p)v\end{pmatrix} \tag{2a}$$

0271-2091/84/080749–16$01.60
© 1984 by John Wiley & Sons, Ltd.
Received 12 November 1982
Revised 1 August 1983

and

$$p = 0{\cdot}4[e - \tfrac{1}{2}\rho(u^2 + v^2)] \tag{2b}$$

ρ is the density, p is the pressure, e is the total energy, u and v are the components of the velocity $\mathbf{V}$.

We may write (1) and (2a) as

$$\frac{\partial W}{\partial t} + \operatorname{div}[H(W)\mathbf{V}] = -\frac{\partial}{\partial x} F_1(W) - \frac{\partial}{\partial y} G_1(W) \tag{3}$$

where

$$H(W) = \begin{pmatrix} \rho \\ \rho u \\ \rho v \\ e + p \end{pmatrix}, \qquad F_1(W) = \begin{pmatrix} 0 \\ p \\ 0 \\ 0 \end{pmatrix}, \qquad G_1(W) = \begin{pmatrix} 0 \\ 0 \\ p \\ 0 \end{pmatrix} \tag{4}$$

Definition of the scheme

As usual we consider a triangulation $\mathcal{T}_h$ of a polygon Ω_h which approximates the domain Ω of integration of (1) (see for example Reference 2). From $\mathcal{T}_h$ we derive a space V_h of functions which are constant on each triangle; the set $\{\pi_T\}_{T \in \mathcal{T}_h}$ is a basis of V_h:

$$\pi_T(x) = \begin{cases} 1 & \text{if } x \in T \\ 0 & \text{elsewhere} \end{cases} \tag{5}$$

Multiplying (3) by π_T and integrating by parts we get, for each triangle T

$$\iint_T \frac{\partial W}{\partial t} \, dx \, dy + \int_{\partial T} H(W)\mathbf{V} \cdot \mathbf{n} \, d\sigma = -\int_{\partial T} [F_1(W)n_x + G_1(W)n_y] \, d\sigma \tag{6}$$

where ∂T and $\mathbf{n} = (n_x, n_y)$ denote, respectively, the boundary of the element T and the (outward pointing) normal vector.

Using the P_0 discretization we get

$$\begin{aligned} W^{n+1}(T) = W^n(T) - \frac{\Delta t}{\text{area}\,(T)} \sum_{c_{ij}}{}' \Big\{ & [\chi_{ij}^n K(W^n(T_{ij})) + (1 - \chi_{ij}^n) K(W^n(T))] \\ & \times \mathbf{V}_{ij}^n \cdot \mathbf{n}^{ij} \text{ length } (c_{ij}) + \frac{F_1(W^n(T_{ij})) + F_1(W^n(T))}{2} n_x^{ij,T} \text{ length } (c_{ij}) \\ & + \frac{G_1(W^n(T_{ij})) + G_1(W^n(T))}{2} n_y^{ij,T} \text{ length } (c_{ij}) \Big\} \end{aligned} \tag{7a}$$

where the superscript n indicates the time level $t = n\,\Delta t$ (Δt is the time increment), the sum $\sum'$ is taken over the three sides c_{ij} of T, T_{ij} denotes the neighbouring triangle of T along the side c_{ij}, $\mathbf{n}^{ij,T} = (n_x^{ij,T}, n_y^{ij,T})$ is the normal vector to side c_{ij} outward from T, and

$$\left.\begin{aligned} \chi_{ij}^n &= 1 \quad \text{if } \mathbf{V}_{ij}^n \cdot \mathbf{n}^{ij,T} < 0 \\ &= 0 \quad \text{otherwise} \end{aligned}\right\} \tag{7b}$$

The upwinding coefficient χ_{ij}^n indicates the element which, between T and T_{ij} is upstream.

Wall (or profile) boundary conditions are simply implemented by computing boundary fluxes with only the pressure terms (using the vanishing of normal velocity); consistent P_0 interpolation is used for the pressure boundary values.

Inflow and outflow boundary conditions are taken into account by imposing all the values at infinity to variables along the boundaries; because of the upwinding, this means that the complete set of four conditions are imposed at inflow, and only the pressure at outflow.

Numerical results

The test presented is the calculation of the steady-state of a *channel transonic flow past a circular bump*: we chose a test problem proposed at the GAMM workshop held in 1979 at Stockholm;[3] this problem has also been tested by Borrel and Morice;[4] the bump is a 4·2 per cent thick circular arc with length 1, and the canal is of height 2·073. Free stream values correspond to a Mach number of 0·85.

For consistency with the GAMM test, we use a triangulation with 72×21 vertices, which gives 2840 triangles (= degrees of freedom); see Figure 1.

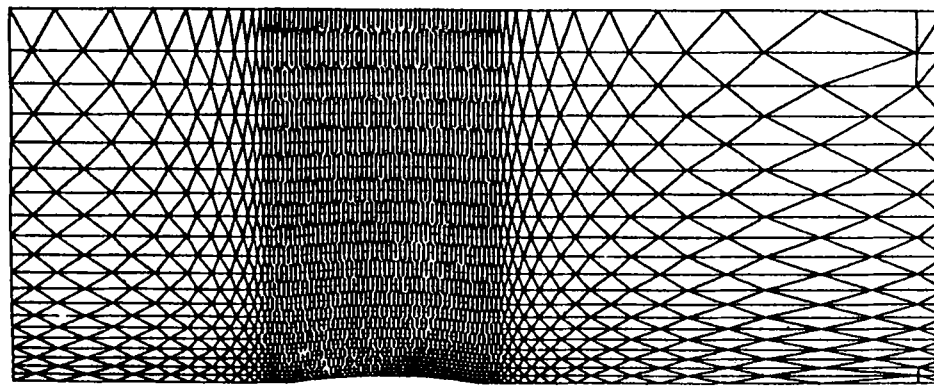

Figure 1. GAMM triangulation: 72×21 vertices

Consistent (not local) time stepping is used, without any artificial damping, to obtain the steady state; convergence is measured from root mean square value of $\partial\rho/\partial t$.

With our method, after 5600 iterations corresponding to time $T = 11{\cdot}6$ s, we have a root mean square value of $\partial\rho/\partial t$, RMS $\partial\rho/\partial t = 0{\cdot}38 \times 10^{-4}$ (Figures 2–4). For the Flic simulation

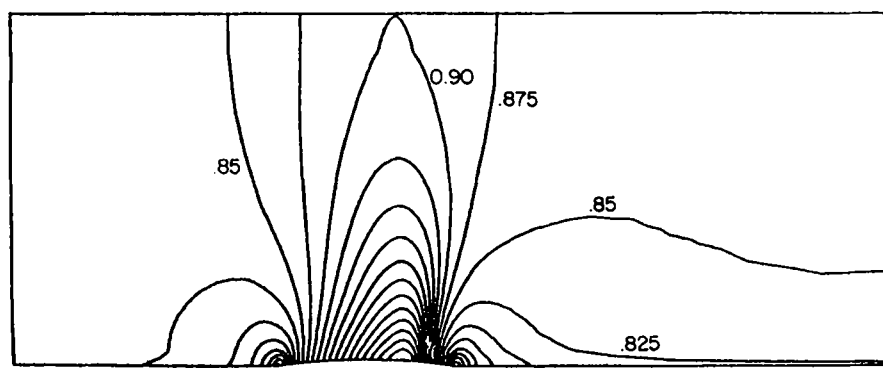

Figure 2. GAMM channel with circular bump; isomach lines. (one step upwind method)

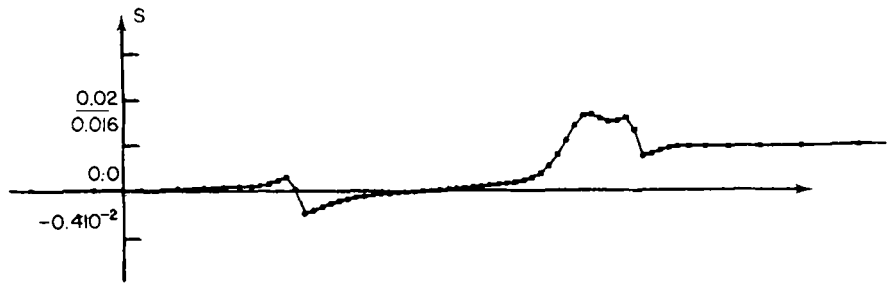

Figure 3. GAMM channel with circular bump; entropy distribution on the bottom (one step upwind method)

described in References 5 and 6, 5600 iterations, $T = 11{\cdot}5$ s correspond to RMS $\partial\rho/\partial t = 0{\cdot}6 \times 10^{-2}$. We observed also that our upwind method is slightly cheaper for each iteration than the Flic method. Our scheme converges in a better manner than the Flic method, but, the results suggest that (Figure 12) the Flic scheme is less diffusive.

Some P_1 variant (Vijayasundaram; unpublished work) of the scheme has been proved to be as expensive with the same number of triangles and much more diffusive.

Figure 4. GAMM channel with circular bump; isentropic lines (increment $\Delta S = 0{\cdot}001$) (one step upwind method)

A RICHTMYER SCHEME

The scalar linear case

Presentation of the scheme. We want to solve the following system

$$\left.\begin{aligned} &\frac{\partial W}{\partial t} + V_1 \frac{\partial W}{\partial x} + V_2 \frac{\partial W}{\partial y} = 0 \text{ in } \mathbb{R}^2 \\ &W(x, 0) = W_0(x) \end{aligned}\right\} \tag{8}$$

where $\mathbf{V} = (V_1, V_2)$ is a constant given velocity.

A classical explicit second-order two-level *time discretization* is the following

$$\begin{aligned} W^{n+1}(x) = W^n(x) &- \Delta t(V_1 W_x^n + V_2 W_y^n) \\ &+ \frac{\Delta t^2}{2}[V_1(V_1(W_x^n + V_2 W_y^n)_x + V_2(V_1 W_x^n + V_2 W_y^n)_y] \end{aligned} \tag{9}$$

Let $\mathcal{H}$ be a set of strictly positive parameters with zero in its closure and let $(\mathcal{T}_h)_{h \in \mathcal{H}}$ be a family of triangulations such that h is the length of the largest segment of $\mathcal{T}_h$. We consider the following spaces

$$H_h = \{v \in L^2(\mathbb{R}^2);\ v \text{ is continuous; } v \text{ is linear on every triangle } T \text{ of } \mathcal{T}_h\}$$
$$V_h = \{v \in H_h \cap H^1(\mathbb{R}^2)\}$$

Then a Galerkin-type variational P_1 space discretization of (9) is

$$\left.\begin{aligned} &W_h^{n+1} \in V_h, \quad \text{and} \quad \forall v \in V_h \\ &\iint (W_h^{n+1} - W_h^n) v \, dx \, dy = -\Delta t \iint v \left(V_1 \frac{\partial W_h^n}{\partial x} + V_2 \frac{\partial W_h^n}{\partial y} \right) dx \, dy \\ &\qquad + \frac{\Delta t^2}{2} \iint \left(V_1 \frac{\partial W_h^n}{\partial x} + V_2 \frac{\partial W_h^n}{\partial y} \right) \left(V_1 \frac{\partial v}{\partial x} + V_2 \frac{\partial v}{\partial y} \right) dx \, dy \end{aligned}\right\} \tag{10}$$

where the sums $\iint$ are taken on $\mathbb{R}^2$.

Since the consistent mass matrix of this discretization is not diagonal, system (10) is expensive to solve in a bounded domain (and impossible to solve in this $\mathbb{R}^2$ case). Following, among others, Ushijima[7] and Baba and Tabata,[8] we construct the mass-lumped variant of (10) by introducing the following notations (h is fixed):

(i) For any vertex A of $\mathcal{T}_h$, the integration zone $\hat{A}$ is defined by dividing the neighbouring triangles into six subtriangles with *median* lines; then the integration zone $\hat{A}$ is the union of those subtriangles which have A as a vertex (Figure 5).

(ii) S_0 is the approximation space of functions which are constant on each $\hat{A}$:

$$S_0 = \{ v \in L^2(\mathbb{R}^2), \, v|_{\hat{A}} = \text{constant}, \, \forall A \text{ vertex of } \mathcal{T}_h \}$$

(iii) $\mathcal{S}_0$ is the trivial projection from H_h to S_0:

$$\left.\begin{aligned} &\forall v \in H_h, \qquad \mathcal{S}_0 v \in S_0 \quad \text{and} \\ &\mathcal{S}_0 v|_{\hat{A}} = v(A), \quad \forall A \text{ vertex of } \mathcal{T}_h. \end{aligned}\right\} \tag{11}$$

Then the mass-lumped variant is

$$\left.\begin{aligned} &W_h^{n+1} \in V_h, \quad \text{and} \quad \forall v \in V_h \\ &\iint \mathcal{S}_0 (W_h^{n+1} - W_h^n) \mathcal{S}_0 v \, dx \, dy \\ &\quad = -\Delta t \iint v \left(V_1 \frac{\partial W_h^n}{\partial x} + V_2 \frac{\partial W_h^n}{\partial y} \right) dx \, dy \\ &\qquad + \frac{\Delta t^2}{2} \iint \left(V_1 \frac{\partial W_h^n}{\partial x} + V_2 \frac{\partial W_h^n}{\partial y} \right) \left(V_1 \frac{\partial v}{\partial x} + V_2 \frac{\partial v}{\partial y} \right) dx \, dy \end{aligned}\right\} \tag{12}$$

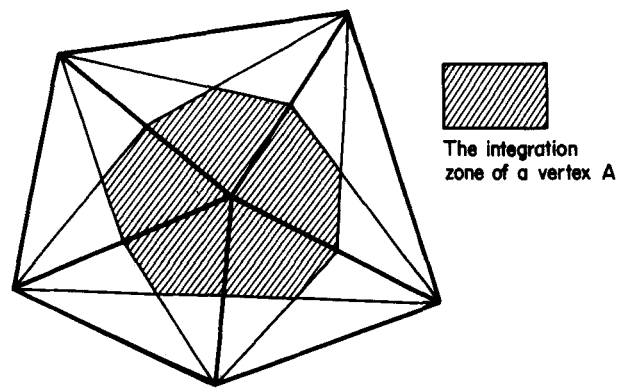

Figure 5. Construction of an integration zone $\hat{A}$ around a vertex A

From the classical results of finite element methods, the right-hand side is second-order accurate; because of the mass-lumping, the left-hand side is only first-order accurate, except for very special regular meshes; see Reference 7 for a discussion of this point in a parabolic context.

However, for nearly or strictly steady simulations (such as transonic ones), the weaker accuracy of the time derivative approximation has less importance.

Let us study the stability of the scheme.

Fourier analysis. For such an analysis, we consider the regular mesh $\hat{\mathcal{T}}_h$ defined as follows:
'*Seven point*' *mesh*: for $(i, j) \in \mathbb{Z}^2$, the triangles of $\hat{\mathcal{T}}_h$ are generated by ($\Delta x = h/\sqrt{2}$):

$$\{[i\,\Delta x, j\,\Delta x], [(i+1)\,\Delta x, (j+1)\,\Delta x], [(i+1)\,\Delta x, j\,\Delta x]\}$$

and

$$\{[i\,\Delta x, j\,\Delta x], [i\,\Delta x, (j+1)\,\Delta x], [(i+1)\,\Delta x, (j+1)\,\Delta x]\}$$

To this triangulation corresponds a seven point approximation (with a seven point cluster) which belongs to the *finite difference* family described by Lerat ([Reference 9, p. 71); by a numerical computation of the extrema of the corresponding amplification factor, we get the *domain of stability* described in Figure 6, the boundary of which intersects the hexagon at points $(0{\cdot}5, 0{\cdot}5)$ and segments $\{-1 \leq x \leq -0{\cdot}481, \ldots, y = 1\}$ and symmetric variants.

Such a diagram leads to the *Courant condition*

$$\|\mathbf{V}\| \frac{\Delta t}{\Delta x} \leq \frac{1}{\sqrt{2}} \tag{13a}$$

but a more general interpretation could be

$$\|\mathbf{V}\| \frac{\Delta t}{\Delta l} \leq 1 \tag{13b}$$

where Δl is the smallest altitude from a given vertex in a neighbouring triangle ('local' Courant condition).

For a non-regular triangulation, (13b) is only a *necessary condition*; to obtain a sufficient one, we shall use an energy argument.

Energy analysis. We shall establish an *a priori* L^2 estimate for the solution (W^n), uniformly with respect to the space increment h; for this purpose, we need some uniform assumptions concerning the triangulations:

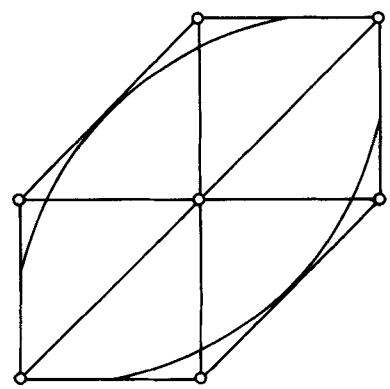

Figure 6. Fourier stability analysis of the 'seven point' finite difference variant

The family $(\mathcal{T}_h)$ of triangulation, h taking all the values in $\mathcal{H}$, is assumed to satisfy

$$\left.\begin{array}{l}\exists K>0 \text{ such that } \forall h\in\mathcal{H}, \forall T\in\mathcal{T}_h,\\ \text{the radii } R(T) \text{ and } r(T) \text{ of respectively circumscribed}\\ \text{and inscribed circles for } T \text{ satisfy}\\ r(T)>\dfrac{h}{K},\quad R(T)/r(T)<K\end{array}\right\} \tag{14}$$

$$\left.\begin{array}{l}\exists K'>0 \text{ such that } \forall h\in\mathcal{H}, \forall T_+ \text{ and } T_-\\ \text{belonging to } \mathcal{T}_h \text{ and having exactly one common}\\ \text{side, we have}\\ \left|\dfrac{\text{area}\,(T_+)-\text{area}\,(T_-)}{\text{area}\,(T_+)}\right|\le K'h\end{array}\right\} \tag{15}$$

Assumption (14) contains a very classical *consistency* one but seems not enough for stability; assumption (15) is quite restrictive as we shall see with the following *example*: we consider the above regular family $(\hat{\mathcal{T}}_h)$ and the following mapping

$$\gamma:\mathbb{R}^2\to\mathbb{R}^2 \qquad \gamma(x,y)=(f(x),y)$$
$$f(x)=\begin{cases}x & \text{if } x\le 0\\ 2x & \text{if } x\ge 0\end{cases}$$

then $(\mathcal{T}_h)=(\gamma[\hat{\mathcal{T}}_h])$ is a family of triangulations with the sides of the triangles suffering some discontinuous variation; $(\mathcal{T}_h)$ does not satisfy (15) (while $(\hat{\mathcal{T}}_h)$ does).

Proposition. Under assumptions (14), (15), *for a discrete initial-condition bounded as follows*

$$\iint |\mathcal{S}_0 W_h^0|^2\,dx\,dy = N<+\infty$$

and for a bounded time interval $[0,T]$, *there exist two real positive constants* $K_1(K',N)$ *and* $K_2(K',N,T,\|\mathbf{V}\|)$ *such that for any* h *in* $\mathcal{H}$, *any* Δt *satisfying the Courant-type condition*

$$\|\mathbf{V}\|\,\Delta t\le K_1\times \textit{smallest length of } \mathcal{T}_h \tag{16}$$

and for any positive integer n *satisfying* $n\,\Delta t<T$, *we have*

$$\iint |\mathcal{S}_0 W_h^n|^2\,dx\,dy\le K_2 \tag{17}$$

Proof. Subscripts h are omitted; we start from (12) with $v=W^{n+1}$ and use the identity $(b-a)b=\frac{1}{2}[b^2-a^2+(b-a)^2]$, together with the notation

$$z=\Delta t\left(V_1\frac{\partial W^n}{\partial x}+V_2\frac{\partial W^n}{\partial y}\right)$$

thus we obtain

$$\begin{aligned}0=&\frac{1}{2}\iint|\mathcal{S}_0W^{n+1}|^2\,dx\,dy-\frac{1}{2}\iint|\mathcal{S}_0W^n|^2\,dx\,dy+\frac{1}{2}\iint|\mathcal{S}_0W^{n+1}-\mathcal{S}_0W^n|^2\,dx\,dy\\&+\iint(W^{n+1}-W^n)z\,dx\,dy+\iint W^n z\,dx\,dy\\&+\frac{1}{2}\iint z\,\Delta t\left(V_1\frac{\partial}{\partial x}+V_2\frac{\partial}{\partial y}\right)(W^{n+1}-W^n)\,dx\,dy+\frac{1}{2}\iint z^2\,dx\,dy\end{aligned}$$

Here we note that the fifth term vanishes; using the fact that medians cut a triangle into six subtriangles with equal areas, we may write the fourth term as follows

$$\iint (W^{n+1} - W^n) z \, dx \, dy = \iint \mathcal{S}_0 (W^{n+1} - W^n) z \, dx \, dy$$

introducing the notation $\theta = W^{n+1} - W^n$, we get

$$\iint |\mathcal{S}_0 W^{n+1}|^2 \, dx \, dy - \iint |\mathcal{S}_0 W^n|^2 \, dx \, dy = -\iint z^2 \, dx \, dy - \iint \theta^2 \, dx \, dy - 2 \iint z\theta \, dx \, dy - I \tag{18a}$$

with

$$I = \iint \Delta t \, z \left(V_1 \frac{\partial \theta}{\partial x} + V_2 \frac{\partial \theta}{\partial y} \right) dx \, dy \tag{18b}$$

First step: computation of spatial derivatives. We need the following additional notations:

(i) For two vertices i and j of a triangle T we denote by

$$\mathbf{n}^{ij,T} = (n_x^{ij,T}, n_y^{ij,T})$$

the normal vector to the side c_{ij} outward from T, and

$$\nu_T^{ij} = \text{length}\,(c_{ij})\, \Delta t (V_1 n_x^{ij,T} + V_2 n_y^{ij,T})$$

(ii) Furthermore, if k is either vertex i or vertex j, the notation $D_{T,k}^{ij}$ denotes the subtriangle of T limited by two medians of T and half of the side c_{ij} which has k as a vertex (Figure 7).

Then we may introduce the following function

$$\alpha : \mathbb{R}^2 \to \mathbb{R}$$

$$\forall D_{T,k}^{ij}, \ \alpha|_{D_{T,k}^{ij}} = \alpha_T^{ij} = \frac{3}{2} \frac{\nu_T^{ij}}{\text{area}\,(T)}$$

and the following relations are easy to verify:

Lemma. (i) *For any side c_{ij} of $\mathcal{T}_h$, we have*

$$\sum_{T = T_i^{ij} \text{ and } T^{ij}} \nu_T^{ij} = 0 \tag{19}$$

where the sum is taken over the two triangles having c_{ij} as a side.

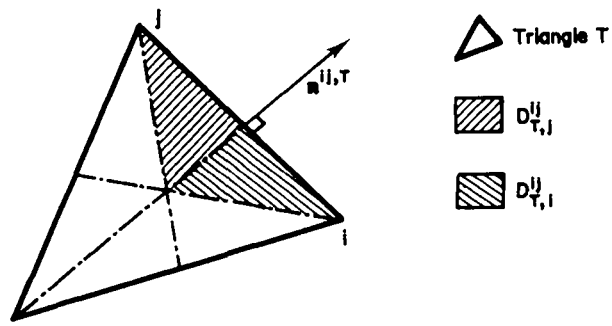

Figure 7

(ii) *For any triangle T of $\mathcal{T}_h$ we have*

$$\sum_{c_{ij}} \nu_T^{ij} = 0 \tag{20}$$

where the sum is taken over the three sides c_{ij} of triangle T.

(iii) *We have*

$$I = 2\iint z\alpha \mathcal{S}_0\theta \, dx \, dy \quad \square \tag{21}$$

Second step. Courant condition. We need now the following condition, which defines K_1:

$$\text{Sup}\,|\alpha| < 1 \tag{22}$$

It is interesting to compare with conditions (13a) and (13b) with the seven point regular mesh; (22) might be roughly interpreted as

$$\|\mathbf{V}\| \frac{\Delta t}{\Delta x} \leq \frac{1}{3\sqrt{2}}$$

which is three times more severe than (13a), but if we denote by Δl_T^{ij} the length of the altitude of T passing by the opposite vertex to c_{ij}, then (22) becomes

$$\frac{\Delta t \mathbf{V} \cdot \mathbf{n}^{ij,T}}{\Delta l_T^{ij}} \leq \frac{2}{3} \tag{23}$$

which, for the seven point case gives

$$\frac{\|\mathbf{V}\| \Delta t}{\Delta x} \leq \frac{\sqrt{2}}{3} \tag{24}$$

However (23) is more interesting with non-regular triangulations, especially if we intend to use some local time stepping. $\square$

Now, the proof in the sequel will be strongly simplified if we reinforce condition (22) as follows

$$|\alpha| \leq 1 - \varepsilon \quad \text{a.e.} \quad \text{in } \mathbb{R}^2 \tag{22'}$$

where ε is an arbitrary small positive constant.

Orientation. From (22) we get $1 + \alpha = [\sqrt{(1+\alpha)}]^2$, and using (21) we have

$$\iint |\mathcal{S}_0 W^{n+1}|^2 \, dx \, dy - \iint |\mathcal{S}_0 W^n|^2 \, dx \, dy = -\iint |\mathcal{S}_0\theta|^2 \, dx \, dy - \iint |z|^2 \, dx \, dy - S_1 - S_2 \tag{25a}$$

with

$$\left.\begin{aligned} S_1 &= 2\iint \sqrt{(1+\alpha)} z v \sqrt{(1+\alpha)} \mathcal{S}_0\theta \, dx \, dy \\ S_2 &= 2\iint \sqrt{(1+\alpha)} z (1-v) \sqrt{(1+\alpha)} \mathcal{S}_0\theta \, dx \, dy \end{aligned}\right\} \tag{25b}$$

where v is a function to be defined in such a manner that (25) is presented as a perturbation of the regular mesh case: the first three terms of the right hand sum represent the regular mesh case: in this case the right-hand side is negative and then the norm $\iint |\mathcal{S}_0 W^n|^2 \, dx \, dy$ is non-increasing with index n, yielding a very strong stability result.

The fourth term S_2 is a remainder to be estimated to yield a (less strong) stability statement for the general case.

Third step: *study of the regular part* S_1. By the Cauchy–Schwarz inequality we get

$$|S_1| \leq \iint (1+\alpha) z^2 \, dx \, dy + \iint v^2 (1+\alpha) \, |\mathcal{S}_0 \theta|^2 \, dx \, dy$$

The first term is easily computed, noting that the function z is constant on each triangle:

$$\iint (1+\alpha) z^2 \, dx \, dy = \sum_{T \in \mathcal{T}_h} z^2(T) \frac{\text{area}\,(T)}{3} \left[3 + \sum_{c_{ij}}' \alpha_T^{ij} \right]$$
$$= \iint z^2 \, dx \, dy$$

here the sum $\sum'$ is taken over the three sides c_{ij} of the triangle T and we used (20).

Let us consider the second term: we note that $\mathcal{S}_0\theta$ is constant on each integration zone $\hat{A}$ (A = vertex); therefore the following decomposition is allowed:

$$\iint v^2 (1+\alpha) \, |\mathcal{S}_0 \theta|^2 \, dx \, dy = \sum_{c_{ij}} \left\{ \iint_{D^{ij}_{T_+ A} \cup D^{ij}_{T_- A}} (1+\alpha) v^2 \, |\mathcal{S}_0 \theta|^2 \, dx \, dy \right.$$
$$\left. + \iint_{D^{ij}_{T_+ A} \cup D^{ij}_{T_- A}} (1+\alpha) v^2 \, |\mathcal{S}_0 \theta|^2 \, dx \, dy \right\}$$

where the sum is taken over *all* the sides c_{ij} of triangulation $\mathcal{T}_h$; T_+ and T_- denote the two triangles having c_{ij} as side. In each of the two integrals of the right hand, $\mathcal{S}_0\theta$ is constant, so that a simplification using (19) will be possible if v *is chosen* to be equal to the function which satisfies the following equality:

$$\iint v^2 (1+\alpha) \, |\mathcal{S}_0 \theta|^2 \, dx \, dy = \iint |\mathcal{S}_0 \theta|^2 \, dx \, dy \tag{26}$$

Summing up, the estimate for S_1 is

$$|S_1| \leq \iint z^2 \, dx \, dy + \iint |\mathcal{S}_0 \theta|^2 \, dx \, dy$$

and (25a) becomes

$$\iint |\mathcal{S}_0 W^{n+1}|^2 \, dx \, dy - \iint |\mathcal{S}_0 W^n|^2 \, dx \, dy \leq |S_2| \tag{27}$$

Fourth step: *study of the remainder* S_2. From (25b) we have (using $|\alpha| \leq 1$)

$$|S_2| \leq 2\sqrt{2} \, \|z\| \, \|\mathcal{S}_0 \theta\| \sup |v\sqrt{(1+\alpha)} - \sqrt{(1+\alpha)}| \tag{28}$$

The following estimate is trivial

$$\|\mathcal{S}_0 \theta\| \leq \|\mathcal{S}_0 W^{n+1}\| + \|\mathcal{S}_0 W^n\|$$

and since z is a linear combination of derivatives of W^n, we obtain

$$|z|^2 \leq \frac{6}{h^2} \|W^n\|^2 \, \|\mathbf{V}\|^2 \, \Delta t^2$$

then it remains to estimate the last factor of (28); now, using (22), (22'), (15) and (26), we see after some easy calculations that

$$\text{Sup} \, |v\sqrt{(1+\alpha)} - \sqrt{(1+\alpha)}| \leq \left(1 + \frac{1}{\varepsilon}\right) K' h$$

So

$$|S_2| \leq 2\sqrt{6}\left(1+\frac{1}{\varepsilon}\right)\|\mathbf{V}\|\,\Delta t K'\{\|\mathscr{S}_0 W^{n+1}\|+\|\mathscr{S}_0 W^n\|\} \tag{29}$$

Fifth step: end of the proof and remarks. From (27) and (29), we have

$$\|\mathscr{S}_0 W^{n+1}\|^2-\|\mathscr{S}_0 W^n\|^2 \leq \Delta t \text{ const } (K', \|\mathbf{V}\|)[\|\mathscr{S}_0 W^{n+1}\|+\|\mathscr{S}_0 W^n\|]$$

from which we derive the strong stability in the sense of Richtmyer and Morton:[10]

$$\begin{aligned}\|\mathscr{S}_0 W^{n+1}\| &\leq [1+\text{const } (K', \|\mathbf{V}\|)\,\Delta t]\|\mathscr{S}_0 W^n\| \\ &\leq \exp[n\,\Delta t \text{ const } (K', \|\mathbf{V}\|)]\|\mathscr{S}_0 W^0\|\end{aligned}$$

and thus we get (17). □

Remark 1. In accordance with Lax's equivalence principle, since both the continuous equations and the discrete scheme are linear, convergence and error estimates can be derived from the above stability study (replacing W^n by the truncature error) and from the consistency assumption (14).

Remark 2. Such explicit finite element stability analysis seems quite rare in the published papers; see however Desgraz and Lascaux's work[11] for a quadrilateral element.

Extension to non-linear systems

The extension to systems is done by a two-step process of Richtmyer type; a choice is made between non-linearly different variants; boundary conditions will be treated either with boundary integrals, or via a different scheme.

The system to be solved is written as

$$\left.\begin{aligned} &W_t+F(W)_x+G(W)_y=0 \\ &+\text{boundary conditions}\end{aligned}\right\} \tag{30}$$

where $W(x, y; t)$ is a vector of $\mathbb{R}^d$.

A natural adaptation of Richtmyer's method is to consider a P_0 (constant by triangle) predictor; similarly to Section 1, we use a control volume formulation for this Lax–Friedrichs' type first step.

According to Lerat and Peyret's study,[12] it is interesting to introduce the length of the first step as a parameter. Then the scheme is the following:

Step 1: *predictor*

$$\left.\begin{aligned} &\forall T \in \mathscr{T}_h, \text{ and for } k=1, 2, \ldots d \\ &\tilde{W}_k(T)=\frac{1}{\text{area }(T)}\left\{\iint_T W_k^n\,dx\,dy-\alpha\,\Delta t\int_{\partial T}[F_k(W^n)n_x+G_k(W^n)n_y]\,d\sigma\right\}\end{aligned}\right\} \tag{31a}$$

Step 2: *Corrector*

$$\left.\begin{aligned} &W^{n+1}\in(V_h)^d, \quad \text{and} \quad \forall \phi \in (V_h)^d, \quad \forall k=1, 2, \ldots, d \\ &\iint_\Omega \mathscr{S}_0\left[\frac{W_k^{n+1}-W_k^n}{\Delta t}\right]\mathscr{S}_0\phi_k\,dx\,dy=\int\!\!\int_\Omega^*\left\{\beta_1\left[F_k(W^n)\frac{\partial\phi_k}{\partial x}+G_k(W^n)\frac{\partial\phi_k}{\partial y}\right]\right. \\ &\qquad\left.+\beta_2\left[F_k(\tilde{W})\frac{\partial\phi_k}{\partial x}+G_k(\tilde{W})\frac{\partial\phi_k}{\partial y}\right]\right\}dx\,dy \\ &\qquad-\int_{\partial\Omega}^*\phi_k[F_k(W^n)n_x+G_k(W^n)n_y]\,d\sigma\end{aligned}\right\} \tag{31b}$$

where

$$\beta_1 = \frac{2\alpha - 1}{2\alpha}, \qquad \beta_2 = \frac{1}{2\alpha}$$

and Ω is the domain of integration of (30).

According to Lerat and Peyret's one dimensional study, we chose the optimal length of the first step:

$$\alpha = 1 + \frac{\sqrt{5}}{2}$$

some experiments with Burgers' equation showed that this choice is advantageous, even for the computation of *stationary shocks.*

Numerical integration is necessary to compute the nonlinear terms:

(a) A rough quadrature is possible for the boundary integral in (31a) because it will be multiplied by Δt^2 in the resulting scheme.

(b) A finer quadrature, exact for P_2 integrands, is used for integrals with stars in (31b).

The last integral of (31b) (boundary fluxes) is not time centred for simplicity; this is only first-order accurate in time; actually second-order spatial accuracy is conserved for steady state simulations. A slightly more expensive variant with a boundary predictor and time centred boundary fluxes has been experimented with, but this brought no noticeable improvements.

Finally, simplified Lapidus type artificial viscosity terms are added for shock resolution, which is a discretization of

$$\chi\left\{\frac{\Delta x^2}{2}\frac{\partial}{\partial x}\left[\left|\frac{\partial W_k}{\partial x}\right|\frac{\partial W_k}{\partial x}\right] + \frac{\Delta y^2}{2}\frac{\partial}{\partial y}\left[\left|\frac{\partial W_k}{\partial y}\right|\frac{\partial W_k}{\partial y}\right]\right\}$$

with the classical choice $\chi = 0{\cdot}8$.

Numerical experiments

For transonic simulations, we had to construct *inflow and outflow boundary conditions*; several extrapolation procedures have been experimented with which failed to give a steady solution for non-regular meshes.

Convergence has been obtained with the use of the following *upwind scheme* for boundary triangles:

For any triangle T such that one vertex at least is inflow or outflow, fluxes between two vertices i and j are computed as integrals along segment CI_{ij} of functions $Fn_x + Gn_y$ (Figure 8) where C is the centroid of triangle T and I_{ij} the middle point of segment C_{ij}.

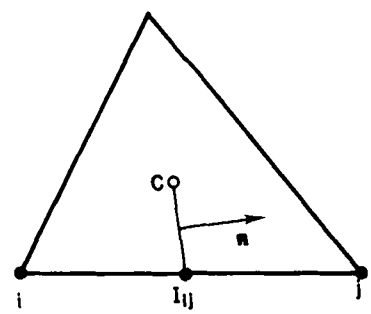

Figure 8. Control volume type flux computation for boundary triangles

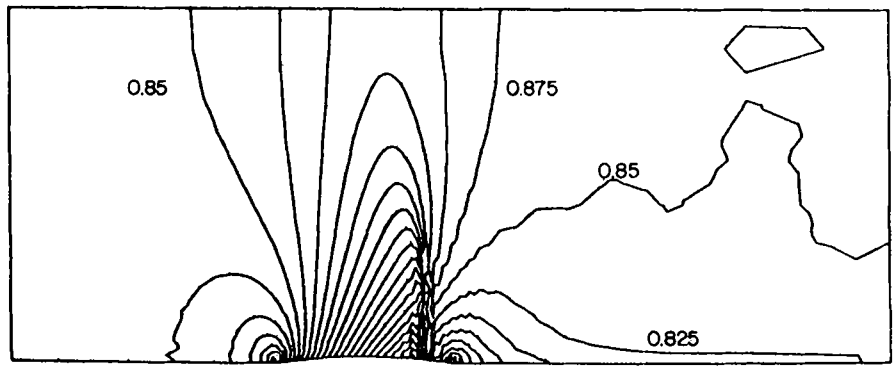

Figure 9. GAMM channel with a circular bump, isomach lines (Richtmyer scheme)

Then two cases are considered for the integration of $Fn_x + Gn_y$:

(i) *First case*: neither i nor j is on the inflow or outflow boundary: the flux through CI_{ij} is computed without using the values of dependant variables at the third vertex.

(ii) *Second case*: vertex i is inflow (resp. outflow) and j is interior (or vice versa): if i is inflow, then it is upstream and j is downstream; if i is outflow, it is downstream and j is upstream; following Lerat and Sides,[13] fluxes are computed by using *upstream values* of the entropy deviation S

$$S = (p/p_\infty)(\rho_\infty/\rho)^\gamma - 1$$

the enthalpy

$$H = \frac{\gamma p}{(1-\gamma)\rho} + \tfrac{1}{2}(u^2 + v^2)$$

and the direction of the flow, and using the *downstream value* of the pressure p.

Summing up, all the four condition at infinity are imposed on inflow and outflow vertices, but only the convenient quantities (three inflow and one outflow) are taken into account by the upwind boundary scheme.

GAMM channel with circular bump. The physical conditions are defined above and the triangulation is the same with 72×21 vertices (= degrees of freedom for each variable).

In the results presented, for the sake of saving cpu time we used a global Courant number and forced the enthalpy

$$H = \frac{\gamma}{\gamma - 1}\frac{P}{\rho} + \tfrac{1}{2}(u^2 + v^2)$$

to have its value at infinity.

We present in Figures 9–11 the isomach and isentropic lines and the entropy deviation distributions on the bottom.

Figure 10. GAMM channel with circular bump; isentropic lines (increment $\Delta S = 0{\cdot}001$) (Richtmyer scheme)

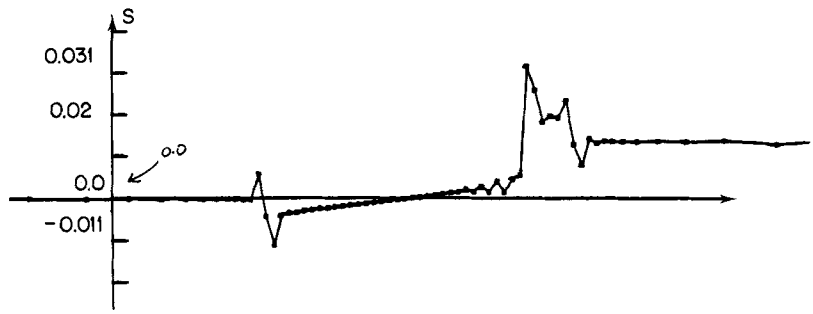

Figure 11. GAMM channel with circular bump; entropy distribution on the bottom (Richtmyer scheme)

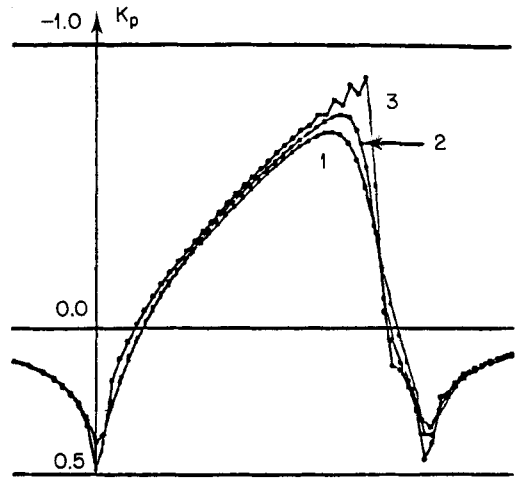

Figure 12. GAMM flow in a channel; comparison of K_p distributions for (1) the one step upwind method, (2) the Flic method, (3) the Richtmyer scheme

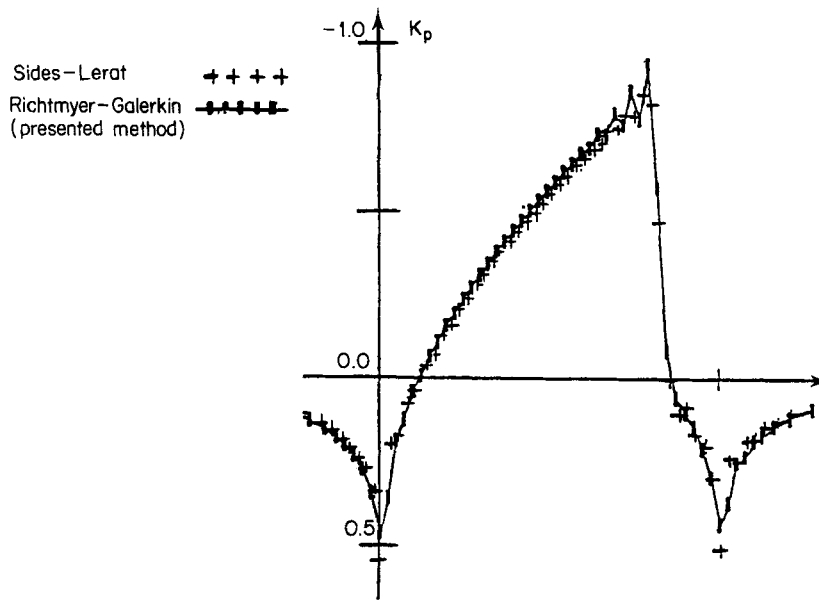

Figure 13. GAMM flow in a channel; comparison of K_p distribution for (1) the Richtmyer scheme and (2) a MacCormack-type scheme by Lerat and Sides[14]

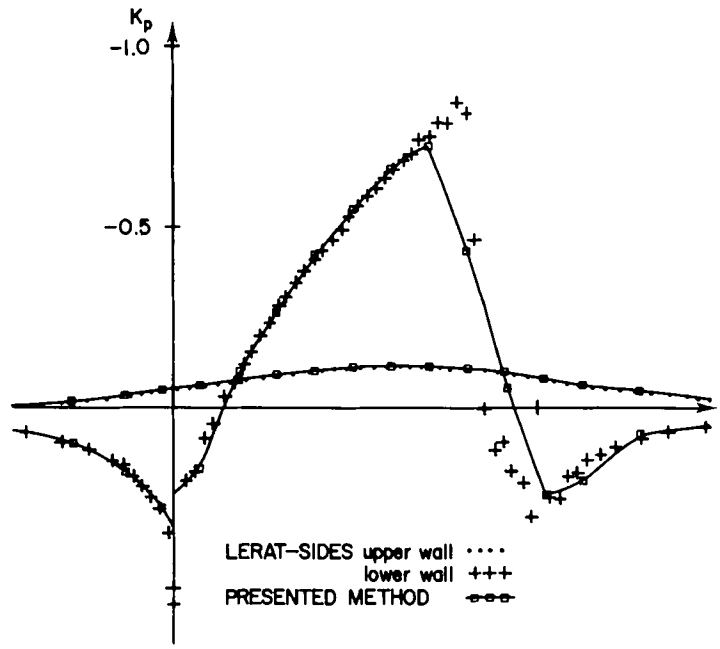

Figure 14. GAMM test with a coarse (151 vertices) triangulation: comparison of K_p distribution of Richtmyer scheme with Lerat and Sides[14]

With an artificial viscosity coefficient equal to 1, some oscillations remain before and after the shock. Results are in good agreement (see Figure 13) with simulations presented by Lerat and Sides,[13,14] and especially with computations with Lerat's seven point optimal S^{α}_{β} scheme (see Reference 9, p. 97, Figure 9b) as could be expected since the scheme presented in this section is quite similar to the latter finite difference scheme. To observe *convergence with respect to mesh spacing, a coarser triangulation* with only 11 nodes along the bump (instead of 41) has been used: a still good agreement is observed, except for the shock capturing, (see Figure 14).

CONCLUSION

Several explicit schemes for *arbitrary finite element triangulations* have been presented to solve Euler equations.

The first-order scheme with convective-type upwinding for F.E.M. is very easy to use. Stationary simulations show shocks captured without oscillations. This scheme is rapidly convergent but quite diffusive.

The second-order Richtmyer scheme is as accurate as several others second order schemes. Thanks to the presence of nodes on the boundaries, extrapolations are needed neither for computation nor for results along the profile. Lerat-type implicit extension (see Reference 9, Chap. 6) is possible.

Several ameliorations are presently studied, such as more sophisticated boundary conditions and artificial viscosity, and higher order F.E.M.

REFERENCES

1. M. O. Bristeau, R. Glowinski, J. Periaux, P. Perrier, O. Pironneau and G. Poirier, 'Transonic flow simulations by finite elements and least square methods', in R. H. Gallagher (Ed.), *Finite Elements in Fluids*, Vol. 4, Wiley, Chichester 1982–1983.
2. O. Zienkiewicz, *The Finite Method in Engineering*, McGraw Hill, Maidenhead, England 1971.
3. A. Rizzi and H. Viviand (Eds), *Numerical Methods for the Computation of Inviscid Transonic Flows with Shock Waves*, Vieweg and Sohn, Braunschweig/Wiesbaden, 1981.
4. M. Borrel, and Ph. Morice, 'A Lagrangian–Eulerian approach to the computation of unsteady transonic flows', *4th GAMM conference*, Paris 7–9 October 1981), *Numerical Methods in Fluid Dynamics*, Vieweg and Sohn, Braunschweig/Wiesbaden (to appear).
5. T. Nagayama and T. Adachi, 'Numerical analysis of flow through turbine cascade by the modified FLIC method', Communicated to *Tokyo Joint Gas Turbine Congress*, 22–27 May 1977, Tokyo, Nagasaki Technical Institute, Mitsubishi Heavy Industries, LTD, Nagasaki, Japan.
6. F. Angrand, V. Boulard, A. Dervieux, J. Periaux and G. Vijayasundaram, 'Transonic Euler simulations by means of finite element explicit schemes', *AIAA Paper* 83–1924 (1983).
7. T. Ushijima, 'Error estimates for the lumped mass approximation', *Memoirs of Numerical Mathematics*, no 6, 65–82 (1979).
8. K. Baba and M. Tabata, 'On a conservative upwind finite element scheme for convective diffusion equations', *R.A.I.R.O. Numerical Analysis*, **15** (1), 3–25 (1981).
9. A. Lerat, '*Sur le calcul des solutions faibles des systèmes hyperboliques de lois de conservation à l'aide de schémas aux différences*', *Thesis*, Paris, 1981.
10. R. D. Richtmyer and K. W. Morton, *Difference Methods for Initial-Value Problems*, Wiley, New York, 1967.
11. J. C. Desgraz and P. M. Lascaux, 'Stabilité de la discrétisation des équations de l'hydrodynamique Lagrangienne 2-D', in R. Glowinski and J. L. Lions (Eds), *Computing Methods in Applied Sciences*, Lecture Notes in Physics 58, Springer, Berlin, 1976, pp. 510–529.
12. A. Lerat and R. Peyret, 'Sur le choix de schémas aux différences du second ordre fournissant des profils de chocs sans oscillation', *Comptes rendus Acad. Sc. Paris, Série A*, **277**, 363–366 (1973).
13. A. Lerat and J. Sides, 'A new finite volume method for the Euler equations with applications to transonic flows', *IMA Conference on Numerical Methods in Aeronautical Fluid Dynamics*, University of Reading, March 1981, to be published by Academic Press.
14. A. Lerat and J. Sides, Contribution to Reference 3.